International Journal of Engineering Research & Technology (IJERT)
ISSN: 2278-0181
Vol. 4 Issue 07, July-2015

Design and Implementation of High-Efficiency Solar Array Simulator by an LLC Resonant Chopper

Ramesh Lakavath
M.Tech (Power Electronics),
Scholar at Prasad Engineering College,
Jangaon, Warangal, Telangana, India

G. Mohan
Associate Professor
Prasad Engineering College
Jangaon, Warangal, Telangana, India

***Abstract*— This Paper proposes a high-efficiency solar array simulator by an LLC resonant chopper to save the cost and energy of photovoltaic system testing. The proposed converter has zero-voltage switching operation of the primary switches and zero-current switching operation of the rectifier diodes. By frequency modulation control, by frequency modulation control, the output impedance of an LLC resonant converter can be regulated from zero to infinite without shunt or serial resistors. Therefore, the efficiency of the proposed solar array simulator can be significantly increased. The circuit operations are analyzed in detail by using simulation and analysis has been done for LLC resonant and the results are proposed.**

Keywords*— LLC resonant chopper, photovoltaic system, solar array simulator

1. INTRODUCTION

With the development of power electronics devices, resonant converter is proved to be more efficient than conventional converter as it employs soft switching technique. Among all renewable energy resources, photovoltaic energy becomes most attractive recently, because it is noiseless, pollution-free, nonradioactive, and inexhaustible. Since the output PV characteristics are influenced by illumination and temperature, the maximum power point tracking is a necessary technology in PV applications. The temperature controlling devices are very expensive, and the power consumption of driving metal-halide lamps results in additional energy waste. Therefore, the literatures propose several solar array simulators which can provide PV characteristics directly. Among them, the most applicable approach in high-power systems is using pulse width modulation (PWM) dc–dc converters to generate PV characteristics. However, shunt resistors are required to limit output voltage at extremely high duty-ratio, and serial resistors are used to inhibit spike current at extremely low duty-ratio operation. These resistors cause additional power dissipations and lower conversion efficiency. Furthermore, the power switches of PWM converters operate in hard switching, which will result in High switching losses and electromagnetic interference issues. Among most resonant converters, the series resonant converter provides satisfied efficiency, but it has the problem of output voltage regulation at light load condition. Although the parallel resonant converter has no light load regulation issue, its circulating energy is much higher than SRC and impacts efficiency significantly. The series-parallel resonant converter remains the advantages of SRC and PRC, which are smaller circulating energy and not so sensitive to load change. However, the same as SRC and PRC, SPRC requires operating at very high switching frequency to obtain extremely low output-voltage. Therefore, with low output-voltage operation, all of SRC, PRC, and SPRC possess high circulating energy to lower their efficiencies.

The LLC resonant converter has smaller circulating energy. Both the active switches of this converter can turn ON with zero-voltage switching, and both the output rectifier diodes can turn OFF with zero-current switching, which results in higher conversion efficiency. By applying frequency modulation control, the output impedance of an LLC converter can be regulated from zero to infinite without shunt or serial resistors hence, the efficiency of the proposed SAS can be significantly increased. By the way, this converter has a transformer to provide electrical isolation for safety requirements.

2. PHOTOVOLTAIC ARRANGEMENTS

2.1 DEFINITION

A photovoltaic system is a system which uses one or more solar panels to convert solar energy into electricity. It consists of multiple components, including the photovoltaic modules, mechanical and electrical connections and mountings and means of regulating and/or modifying the electrical output

2.2 PHOTOVOLTAIC CELL

PV cells are made of semiconductor materials, such as silicon. For solar cells, a thin semiconductor wafer is specially treated to form an electric field, positive on one side and negative on the other. When light energy strikes the solar cell, electrons are knocked loose from the atoms in the semiconductor material. If electrical conductors are attached to the positive and negative sides, forming an electrical circuit, the electrons can be captured in the form of an electric current - that is, electricity. This electricity can then be used to power a load. A PV cell can either be circular or square in construction

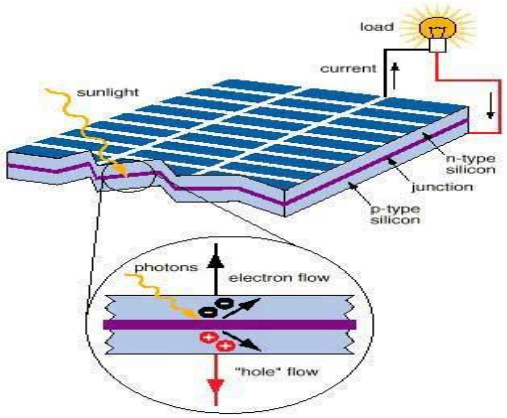

Figure 1 Basic Structure of PV Cell

2.3 PHOTOVOLTAIC MODULE

Due to the low voltage generated in a PV cell (around 0.5V), several PV cells are connected in series (for high voltage) and in parallel (for high current) to form a PV module for desired output. Separate diodes may be needed to avoid reverse currents, in case of partial or total shading, and at night. The p-n junctions of mono-crystalline silicon cells may have adequate reverse current characteristics and these are not necessary. Reverse currents waste power and can also lead to overheating of shaded cells. Solar cells become less efficient at higher temperatures and installers try to provide good ventilation behind solar panels

2.4 PHOTOVOLTAIC ARRAY

The power that one module can produce is not sufficient to meet the requirements of home or business. Most PV arrays use an inverter to convert the DC power into alternating current that can power the motors, loads, lights etc. The modules in a PV array are usually first connected in series to obtain the desired voltages; the individual modules are then connected in parallel to allow the system to produce more current

2.5 MAXIMUM POWER POINT TRACKER

Maximum power point controller, can track the maximum power of an array quickly without perturbation and observation process but also can be implemented easily. The main idea is based on the graphical interpretation of the maximum power point as the intersecting point of two curves on the phase plane corresponding to the solution of two algebraic equations. In other words, the operating point is the intersecting point of the PV-array characteristic curve and the maximum power line. Due to the high initial installation cost and the low energy conversion efficiency, a maximum power point tracking (MPPT) control for the solar array is essential in a photovoltaic power system.

Various methods of MPPT control have been proposed in existing literature, they can be roughly classified into two categories. One belongs to the perturbation and observation method by periodically increasing or decreasing the array voltage to approach the maximum power point. The other belongs to the incremental conductance methods by comparing with the instantaneous static conductance to locate the maximum power point quickly. It is seen that the first category usually fails to quickly track the maximum power while the second one requires complicated implementation.

3. LLC RESONANT CHOPPER

The circuit diagram of an LLC resonant chopper is shown in Fig. 6, which consists of an LLC resonant inverter, a current-driven transformer with a center-tapped rectifier. The topology of LLC converter is very similar to that of SRC. The main difference is that the magnetizing inductance L_m is only slightly higher than the resonant inductance L_r in the LLC converter. Therefore, at some load conditions, Lm may participate in the resonance with L_r and C_r and change the characteristics of resonant tank.

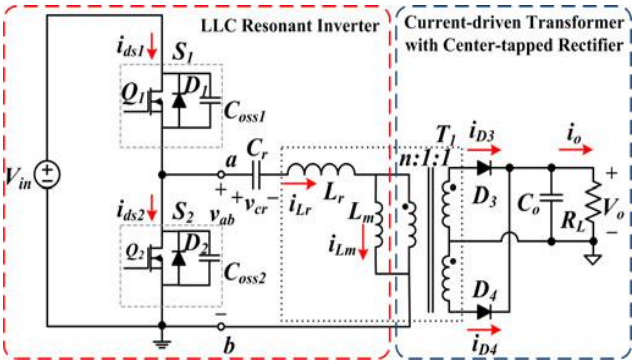

Figure 2 Circuit diagram of LLC resonant chopper

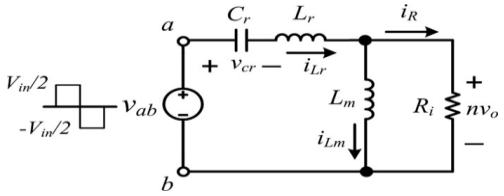

Figure 3 Equivalent circuit of the LLC resonant converter.

The equivalent circuit of the LLC resonant inverter can be depicted as shown in Fig. 3, in which R_i is equivalent load resistance seen in primary side, and can be expressed as R_i = 8n2RL /π2 . The input symmetrical square waveform v_{ab} with the magnitude of $V_{in}/2$ can be obtained by alternate conducting of power switches S_1 and S_2. The transfer function of output voltage can be determined as (5) shown at the bottom of the next page, where the inductance ratio A, the second resonant frequency ωL, and the load quality factor Q_L are defined as

$$A = \frac{L_r}{L_m} \quad ----------(1)$$

$$wL = 2\pi fL = \frac{1}{\sqrt{L_r + L_m}} \quad -----(2)$$

$$QL = R_i \times \sqrt{\frac{C_r}{L_r + L_m}} = R_i . \omega_l . C_r \quad --(3)$$

The frequency response of output voltage gain of the LLC resonant converter can be illustrated in Fig. It can be observed that there are two resonant frequencies. The second resonant frequency and the main resonant frequency ω_H can be determined as follows:

$$\omega_H = 2\pi f_H = \frac{1}{\sqrt{L_r \cdot C_r}} - - - - - (4)$$

Fig. 4 can be divided into three operation regions according to the resonant frequencies of and . Because the impedance of resonant tank is capacitive in Region 3, the primary switches can operate under ZCS condition. But the current spike during turn-on transient will result in high-current stress and high-switching loss. Therefore, LLC resonant converters should be prevented from operating in this region.

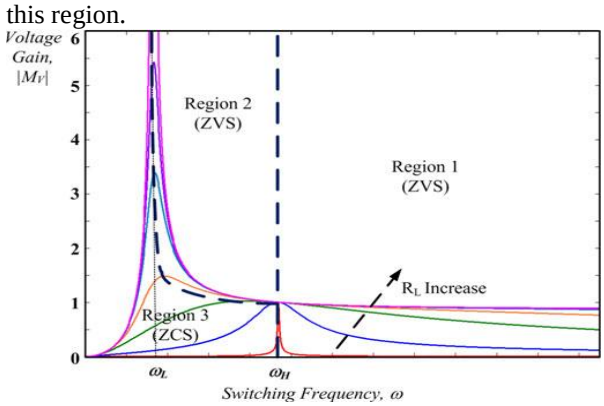

Figure 4 Frequency response of output voltage gain of the LLC resonant converter.

In region 1, the switching frequency is higher than the resonant frequency . The impedance of resonant tank is inductive so that the switches can operate under ZVS condition to reduce switching loss. Since voltage gain is always less than 1, the converter could be regarded as buck type. The operation principle in this region is very similar to SRC; hence, secondary rectifier diodes cannot operate under ZCS. Voltage spike will occur during turn-off transient and results in high switching loss.

According to Fig. 4, the switching frequency is lower than the main resonant frequency in region 2, in which the converter is regarded as boost type (voltage gain ≥ 1). During the main resonant period, because the voltage of Lm is clamped by output voltage, the inductor current i_{Lm} is linearly increasing. While reaches the same level as the resonant current, a second resonance with the frequency determined by Cr and (Lr + Lm) occurs. This resonance will continue until the primary switches switching again so that the converter can still operate under ZVS in region 2. Besides, during the second resonant period, the current of secondary rectifier diodes remains zero; hence, they can turn OFF naturally under ZCS condition.

Theoretically, the optimal converter efficiency should be obtained in the point of switching frequency equal to the second resonant frequency . For practical considerations, in order to minimize power dissipation of SAS and prevent the operation point from entering region 3, the switching frequency of SAS operating in maximum output power should be designed as slightly higher than resonant frequency .

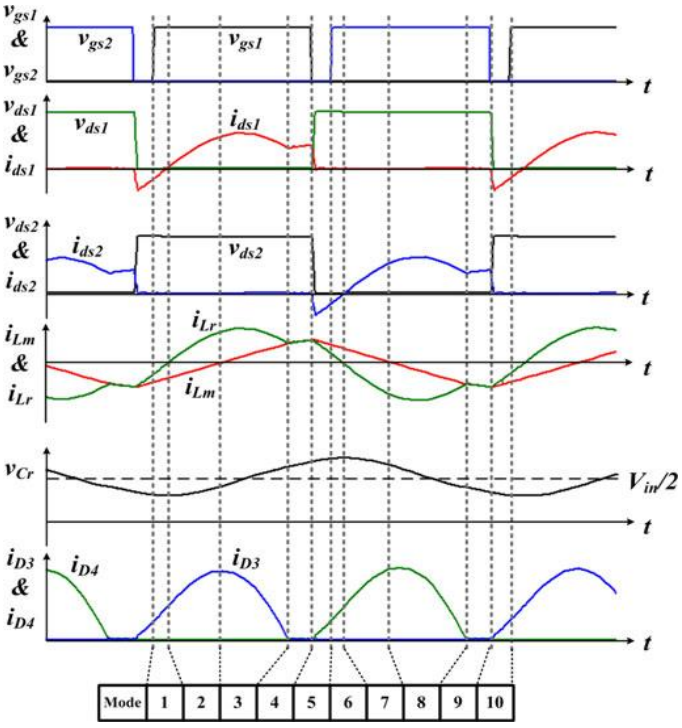

Figure 5 Main waveforms of the LLC resonant converter operating.

4. PRINCIPLE OF OPERATION LLC RESONANT DC-DC CONVERTER

The primary switches S_1 (S_2) are composed of an MOSFET Q_1 (Q_2), and its intrinsic anti parallel diode D1 (D2) and equivalent output capacitor C_{OSS1} (C_{OSS2}). The resonant tank is formed by the resonant capacitor C_r, and the leakage inductor and magnetizing inductor L_m of the transformer T_1. By conducting the switches S_1 and S_2 alternately, a symmetrical square waveform with the magnitude of /2 can be obtained in the input terminal of the resonant tank, where V_{in} is the input voltage. The center-tapped rectifier is constructed by connecting diodes D_3 and D_4 to the secondary windings of T_1. Based on the analysis of earlier section, the main theoretical waveforms of the LLC resonant converter operating in region 2 are shown in Fig. 5. There are ten operation modes within one switching period. Because the waveforms are symmetrical, only the operation principles of the first five modes are introduced referring to the equivalent circuits.

A. Mode 1

This mode starts when the switch S_1 is turned ON under ZVS. The equivalent circuit is shown in Fig. 6(a). The resonant current is sine-wave and increases from negative to discharge C_r, and energy returns to the input voltage source. The voltage of L_m is clamped to so that the magnetizing current increases linearly from negative. The

energy stored in Lm will be released through D_3 to output load. When reaches zero, this mode ends.

B. Mode 2

As shown in Fig. 6(b), since i_{Lr} increases from zero to positive, the input voltage source charges C_r and L_r , and supplies energy to output load simultaneously. The energy in L_m is released to output load continuously. When i_{Lm} reaches zero, this mode ends.

C. Mode 3

At this mode, because the voltage of Lm is still clamped to nV_O, i_{Lm} remains increasing linearly. The input voltage source charges Lm and supplies energy to output load. The equivalent circuit is shown in Fig. 6(c).

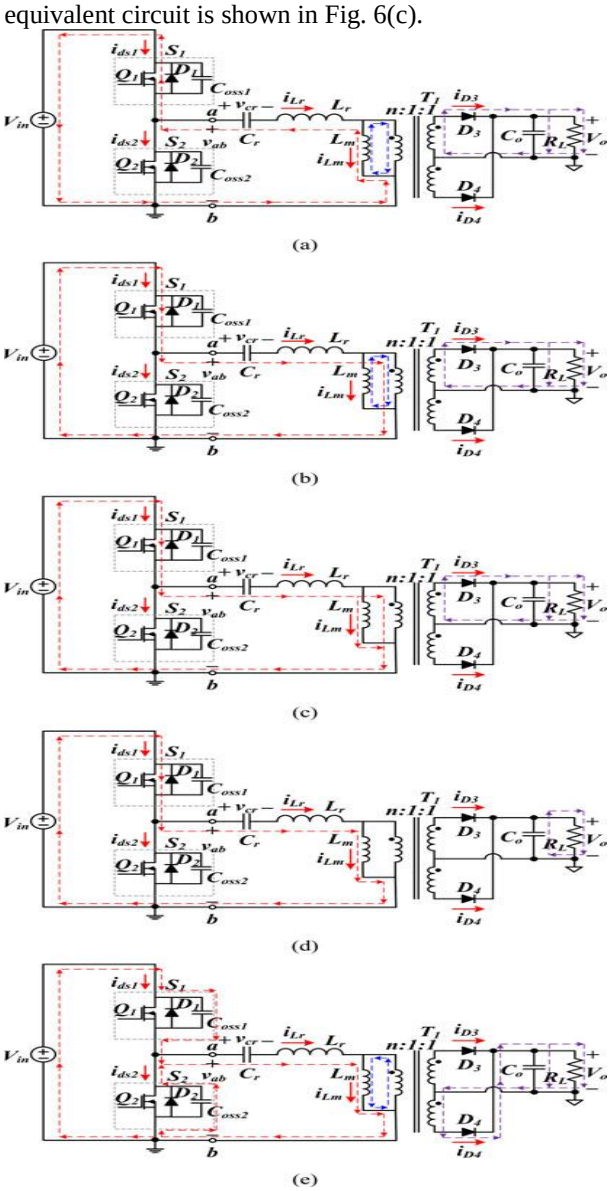

Figure 6 : Equivalent circuits of (a) Mode 1, (b) Mode 2, (c) Mode 3, (d) Mode4, and (e) Mode 5 for the LLC converter operating in region 2.

D. Mode 4

This mode starts when i_{Lr} and i_{Lm} equal each other. Current circulating through the secondary diode D_3 naturally decreases to zero so that this diode turns OFF under ZCS condition. The voltage spike caused by diode reverse recovery would not exist. The voltage of Lm is no longer clamped to , hence, Lm is in series with Lr and participates in the resonance with Cr. The equivalent circuit of this mode is shown in Fig. 6(d). Because the equivalent inductance of (Lr + Lm) is higher than Lr, as shown in Fig. 9, and are almost constant in this short time interval.

E. Mode 5

As shown in Fig. 6(e), while S_1 is turning OFF, the resonant current charging C_{OSS1} and discharging C_{OSS2} simultaneously. At the moment of vds2 decreasing to zero, the resonant current flows through anti paralleled diode D_2 which provide ZVS operation for S_2 turn ON. At the same time, the secondary rectifier diode D_4 turns ON. The voltage of Lm is clamped to reverse polarity so that the current becomes decreasing linearly. The magnetizing inductor Lm is separated from the resonance with Cr .When S_2 turns ON under ZVS; this mode ends and enters the half cycle with symmetrical operation principles.

5. EXPERIMENTAL RESULTS

Based on the previous design, the electrical specifications and component parameters of the *LLC* resonant converter are summarized in Table II. For convenience to explain the experimental results, the theoretical *V–I* curve of F-MSN-75W-R-02 at 80mW/cm^2 and 25˚C is shown in Fig. 9(a), in which the dots, from "A" to "H," indicate operation points in this curve. By the way, all points are also depicted in the frequency response of output voltage, as shown in Fig. 9(b). It can be observed that points "D," "E," and "F" are located in region 2 to obtain high efficiency in high output-power operations.

Fig. 7 shows the voltage and current waveforms of the primary switches S1 and S2, when the SAS operates at the maximum power point (MPP) (point "E") and two extreme points (points "A" and "H"), respectively. They could be observed that S1 and S2 can turn ON under ZVS condition at all operation conditions. Besides, when the SAS operates at point "E" with high-output power, the turn-off current can be reduced by the second resonance, as shown in Fig. 10(a). Therefore, the circulating energy and turn-off loss can be significantly minimized to improve system efficiency.

TABLE II
ELECTRICAL SPECIFICATIONS AND COMPONENT PARAMETERS OF THE ILLUSTRATIVE EXAMPLE

Electrical Specifications	
Input Voltage, V_{in}	400V
Output Voltage, V_O	0 – 21V
Output Current, I_O	0 – 4A
Maximum Power, P_O	60W
Main Resonant Frequency, f_H	100 kHz
Secondary Resonant Frequency, f_L	57.7 kHz
Switching Frequency	60 – 250 kHz
Component Parameters	
Resonant Inductor, L_r	650 µH
Magnetizing Inductor, L_m	1.3 mH
Resonant Capacitor, C_r	3.9 nF
Transformer Turn Ratio, n:1:1	14:1:1
Primary Switch, S_1 and S_2	STP10NK60Z
Rectifier Diode, D_3 and D_4	STPS3045CW

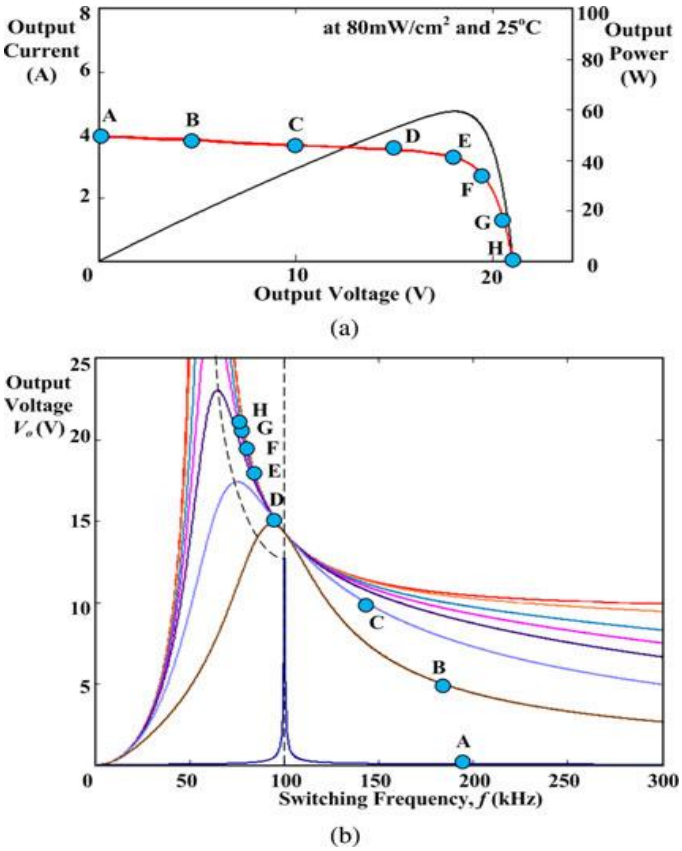

Figure 7 :. Related operation points indicated in (a) the V–I curve and (b) the frequency response of output voltage

Fig. 8 shows the measured efficiencies according to the Operation points (from "A" to "H") marked at the theoretical V–I curve. The maximum system efficiency is up to around 92.5% and occurs at the MPP "E," resulting in energy saving significantly.

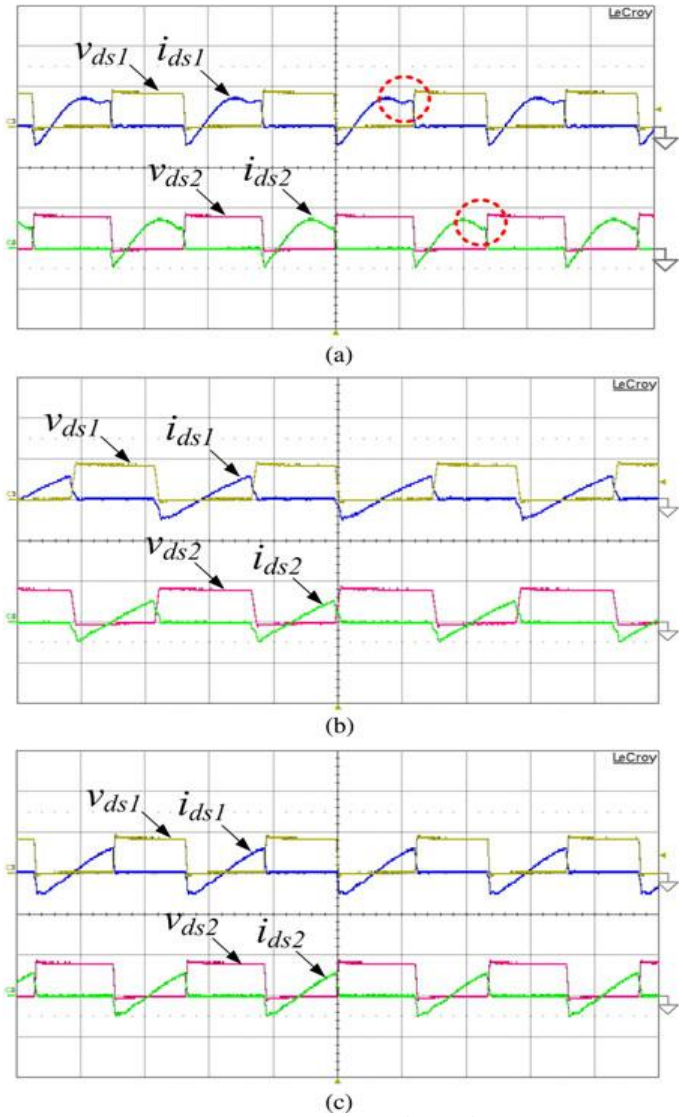

Figure 8 Measured voltage and current waveforms of primary switches S1 and S2 when the proposed SAS operates at (a) point "E" (vds1, vds2 : 500 V/div; ids1 , ids2 : 1 A/div; time: 5µs/div), (b) point "A" (vds1 , vds2 : 500 V/div; ids1 , ids2 : 1 A/div; time: 2

The measured transient response to the step changes between the operation points of "E" and "G." It can be observed that the output voltage can vary according to the corresponding output current and returns to steady state within 6 ms. Fig. 13 shows the measured V–I curve of the proposed SAS with closed-loop control. It can be observed that the measured output characteristics are very close to the theoretical V–I curve obtained from (3). These results prove that the output voltage and current of the proposed SAS can be adjusted simultaneously to match the electrical characteristics of PV output.

In order to further verify the system stability, a boost converter with perturb and observe (P&O) MPPT algorithm and output-current feedback control is connected in series with the proposed SAS. This is one of the most popular structures to achieve MPPT feature in the PV applications. The measured frequency responses of the SAS output impedances Z_o are shown in Fig. 14, in which the curves are measured according to the operation points of "D," "E," and

"F." As discussed in the literature [23], the impedance ratio, defined as *Tm* = *Zo*/Zin , can be used to determine the system stability, where Zin is the input impedance of the boost converter. By comparing the frequency responses of *Zo* with those of *Z*in , the simulated frequency response of *Tm* can be illustrated in Fig. 15. It reveals that the gain |*Tm*| is always less than 0 dB between 1 Hz and 100 kHz so that this cascaded system can operate stably in this frequency range. Furthermore, Fig. 16 shows the measured waveforms of *iLr* , *vo* , *io* , and *Po* of the proposed SAS while the boost converter starts up and then tracks the MPP. This result validates the ability of the proposed SAS for stable operation with an authentic MPPT converter.

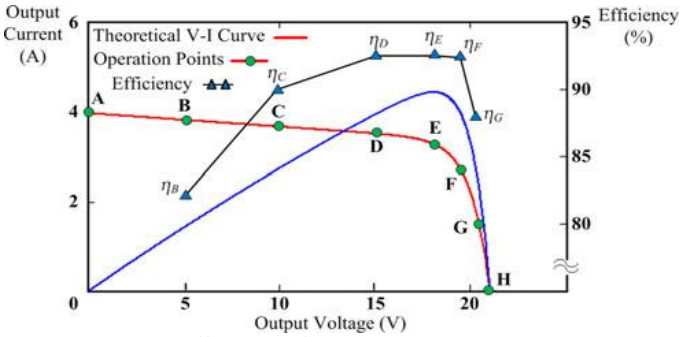

Figure 9 Measured efficiencies of the proposed SAS according to the operation points "A" to "H."

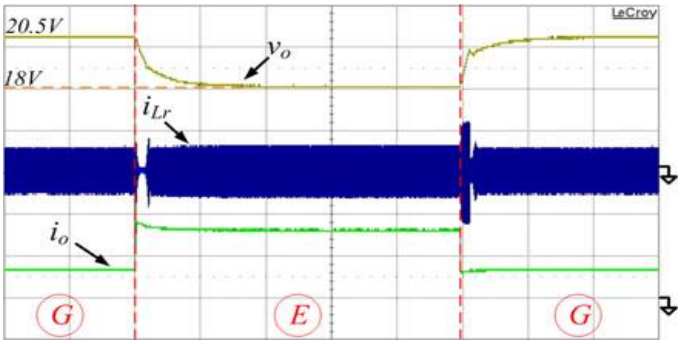

Figure 10 Measured transient response to the step changes between the operation points of "E" and "G" (vo : 2 V/div; io : 2 A/div; iLr : 1 A/div; time: 5 ms/div).

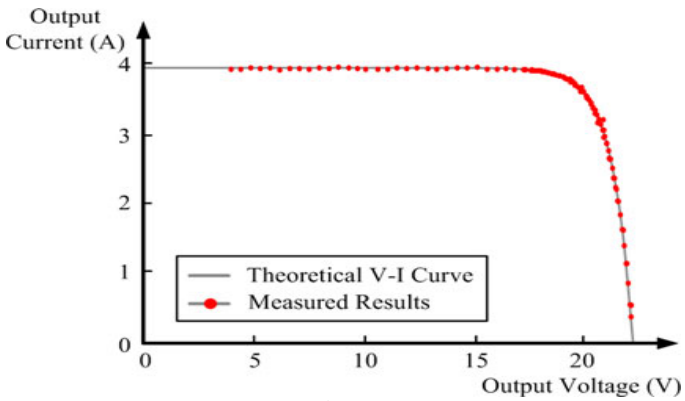

Figure 11 Measured V–I curve of the proposed SAS with closed-loop control.

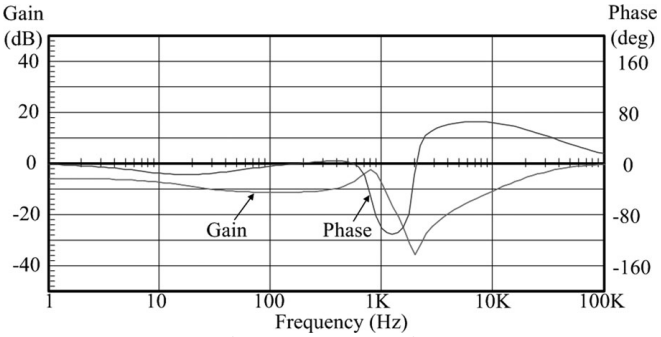

Figure 12 Simulated frequency response of the impedance ratio Tm.

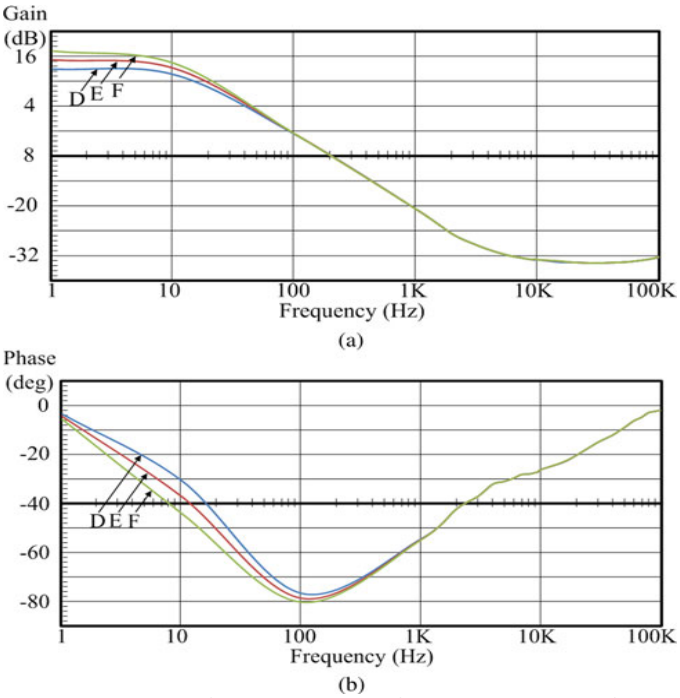

Figure 13 Measured frequency responses of (a) gain and (b) phase of the SAS output impedances Zo

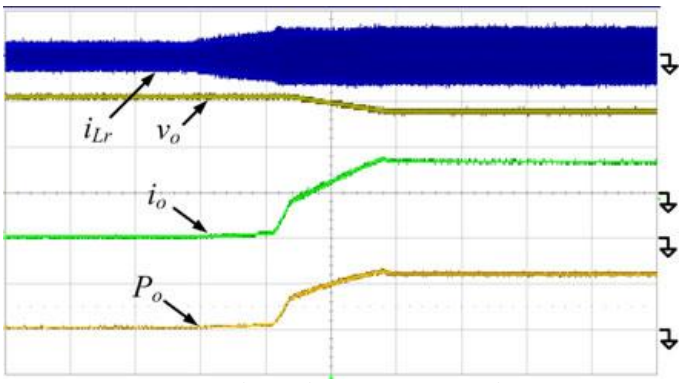

Figure 14 Measured waveforms of iLr, vo , io, and Po of the proposed SAS while the boost converter starts up and then tracks the maximum power point(vo:10 V/div; io :2 A/div; iLr :1 A/div; Po : 50 W/div; time: 500 ms/div).

1. *SIMULATION CIRCUIT FOR SAS BY ANLLC RESONANT INTERFACING OF THE SAS WITH LLC RESONANT DC-DC CONVERTER*

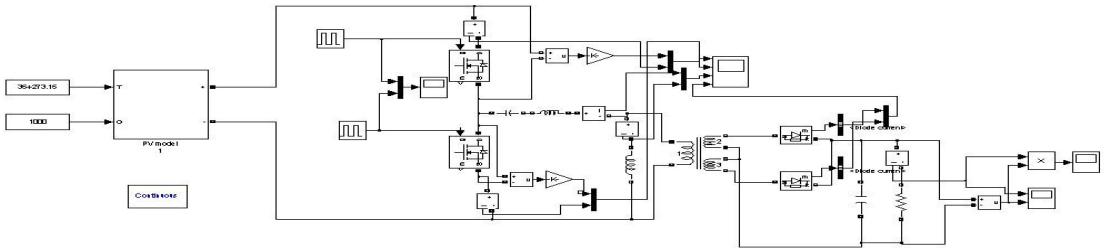

Figure 15 The complete simlink circuit model showing the coupling of PV array with the LLC Resonant DC-DC converter

2. SIMULATION RESULTS

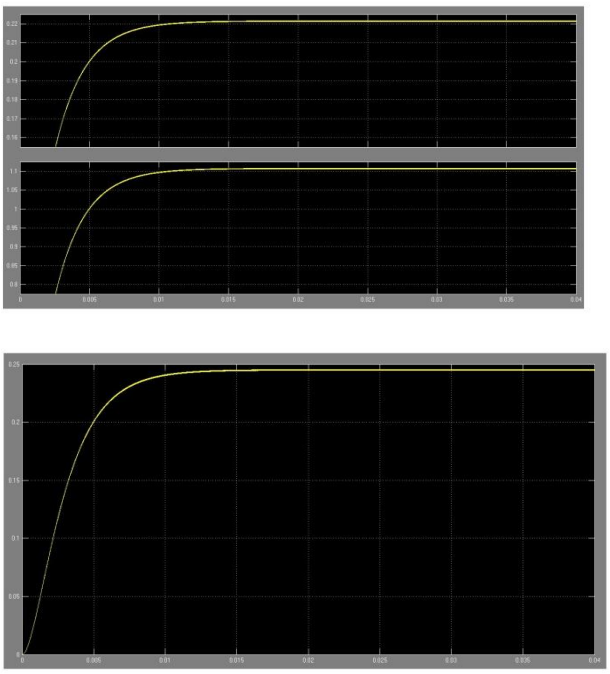

Figure 16 V-I WAVEFORM

3. CONCLUSION

A reliable and simple scheme integrating wind-driven induction generators and PV array has been successfully developed for the first time to supply a three-phase remote load with constant frequency balanced voltages. The generation system will supply constant voltages with varying wind speed and irradiation when the battery is switched on. The hybrid system is cost-effective and requires a simple interface for integration, thus making it suitable for off-grid applications. The independent control of real and reactive power supplied to the load is achieved with the help of SRF theory along with the load balancing, load compensation and harmonic distortion compensation.

A dc–dc step-up converter can be interposed in the proposed system between the PV array and the inverter to maintain the PV array voltage constant for varying atmospheric conditions. The same converter can track the peak-power point of the PV array when the battery is switched to the system.

4. REFERENCES

[1] Rui Yang, HongFa Ding, Yun Xu, Lei Yao, and YingMeng Xiang, "An Analytical Steady-State Model of LCC type Series–Parallel Resonant Converter With Capacitive Output Filter" *IEEE Trans.Power Electron*, VOL. 29, NO. 1, Jan 2014

[2] Ahmed A. Aboushady, Khaled H. Ahmed,Stephen J. Finney, and Barry W. Williams "Linearized Large Signal Modeling, Analysis, and Control Design of Phase-Controlled Series-Parallel Resonant Converters Using State Feedback" *IEEE Trans.Power Electron*, VOL. 28, NO. 8, Aug 2013

[3] Chien-Hsuan Chang, En-Chih Chang, and Hung-Liang Cheng, "A high-efficiency solar array simulator implemented by an LLC resonant DC–DC converter," *IEEE Trans. Power Electron*, VOL. 28, NO. 6, Jun 2013

[4] Thiago B. Soeiro, Jonas Mühlethaler, Jörgen Linnér, Per Ranstad, and Johann W. Kolar, "Automated Design of a High-Power High-Frequency LCC Resonant Converter for Electrostatic Precipitators" " *IEEE Trans.Power Electron* VOL. 60, NO. 11, Nov 2013

[5] Ying-Chun Chuang, Yu-Lung Ke, Hung-Shiang Chuang, and Jung-Tai Chen "A Novel Loaded-Resonant Converter for the Application of DC-to-DC Energy Conversions" *IEEE Trans. Industry Applications*, VOL. 48, NO. 2, Mar/Apl 2012

[6] D. G. Infield, G. W. Slack, N. H. Lipman, and P. J. Musgrove, "Review of wind/diesel strategies," *Proc. Inst. Elec. Eng. A*, vol. 130, no. 9, pp.613–619, 1983.